APPENDIX A

Detailed Model: Concentric Tube Counterflow Heat Exchanger

A detailed model was written for a concentric tube counterflow heat exchanger. Following is a description of the model, and a short presentation of simulation results using the model.

A.1 Geometry

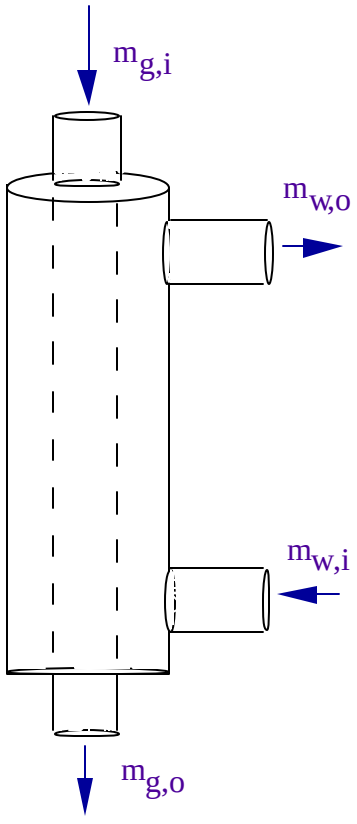

Figure A.1 Side view of concentric tube counterflow heat exchanger.

For the correlations that follow, the only geometric variables of concern are the hydraulic diameter and the free flow area. The hydraulic diameter of a concentric tube heat exchanger is found using:

$$D_H = D_o - D_i \tag{A.1}$$

where D_o and D_i are the inner shell and inner tube diameters respectively.

The free flow area is found using:

$$A_F = \frac{1}{4}\pi\left(D_o^2 - D_i^2\right) \tag{A.2}$$

A.2 Heat Exchanger Shear Pressure Drop

For concentric tube geometries, turbulence occurs for Reynolds numbers greater than 2300 (Kakic 1987). For the low flow rates expected in concentric tube heat NCHEs, it may be assumed that the flow will remain laminar. The velocity of the water stream can be found using:

$$v_w = \frac{\dot{m}_w}{\bar{\rho}_{HX,w} A_F} \tag{A.3}$$

where $\bar{\rho}_{HX,w}$ is the average water density in the heat exchanger. The Reynolds number is calculated using:

$$\mathrm{Re}_D = \frac{\bar{\rho}_{HX,w} v_w D_H}{\bar{\mu}_{HX,w}} \tag{A.4}$$

The Fanning friction factor for concentric tubes is found using the correlation (Kakic 1987):

$$f\,\mathrm{Re}_D = \frac{16\left(1-r^*\right)^2}{1+\left(r^*\right)^2 - 2\left(r_m^*\right)^2} \tag{A.5}$$

$$\textit{where} \qquad r^* = \frac{D_i}{D_o} \tag{A.6}$$

$$r_m^* = \sqrt{\frac{1 - r^*}{2 \ln\left|\frac{1}{r^*}\right|}} \tag{A.7}$$

The shear pressure drop in the heat exchanger is found using the relationship:

$$\Delta P_{HX,sh} = f \frac{4 L_{HX}}{D_H} \frac{1}{2} \overline{\rho}_{HX,w} v_w^2 \tag{A.8}$$

where L_{HX} is the length of the heat exchanger. The minor loss entrance and exit conditions were found as described in Section 4.2.1.

A.3 Heat Exchanger Heat Transfer

A modified effectiveness-NTU approach was taken to calculate the heat transfer in the concentric tube heat exchanger. The modeling method used resembles the method described in Section 4.2.1. The only change in the modeling lay in the finding of heat transfer coefficients.

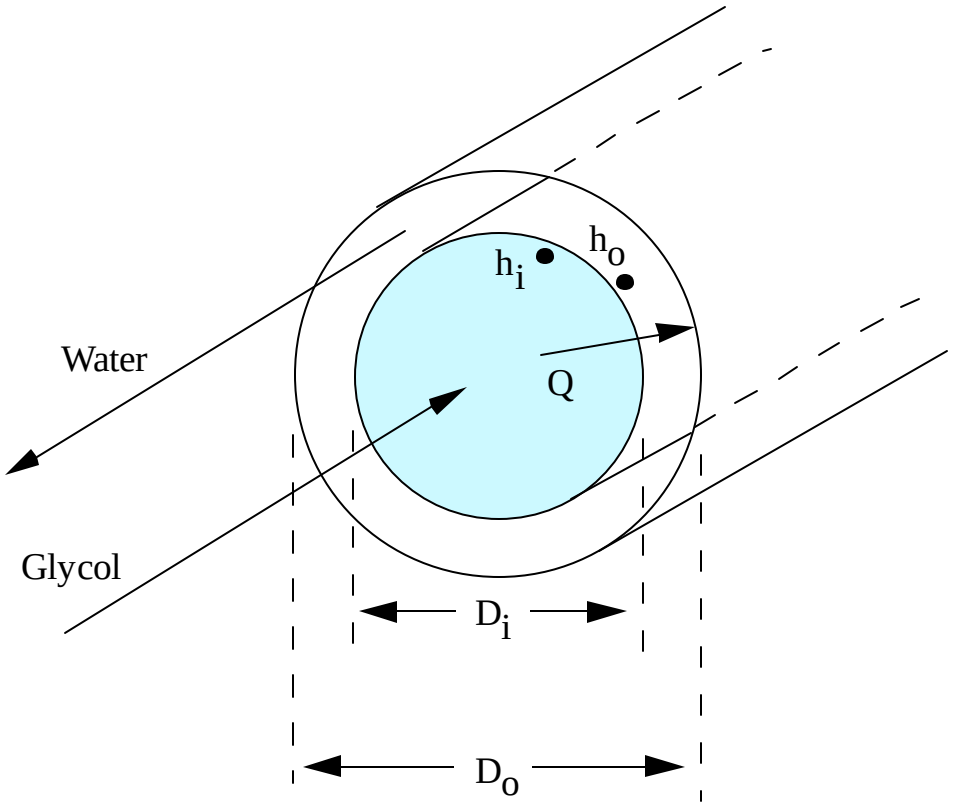

Figure A.2 Locations of heat transfer coefficients in concentric tube counterflow NCHE.

Assuming laminar flow, and uniform heat flux, the Nusselt number for the inner glycol-filled tube is of the form:

$$Nu_{D,i} = 3.66 \qquad \text{(A.9)}$$

Although mixed convection will be experienced in the heat exchanger, the following analysis assumes only forced convection. For fully developed, laminar water flow in a circular tube annulus with the outer surface insulated and the inner surface at constant temperature, the Nusselt number can be found in Table A.1 as a function of r* (Incropera and DeWitt 1985).

Table A.1 Nusselt number for fully developed laminar flow in a circular tube annulus with outer surface insulated and inner surface at constant temperature

r*	$Nu_{D,o}$
0	-
0.005	17.46
0.1	11.56
1.25	7.37
1.5	5.74
1.0	4.86

The heat transfer coefficient for the annulus can be found using the hydraulic diameter:

$$h_o = \frac{Nu_{D,o}\,\bar{k}_w}{D_H} \qquad \text{(A.10)}$$

where the hydraulic diameter is found using:

$$D_H = D_o - D_i \qquad \text{(A.11)}$$

A.4 Comparison of Concentric Tube Counterflow Simulation Results to Shell and Coil Simulation Results

Simulations were performed employing the detailed concentric tube counterflow model, and are compared to simulation results for the Thermo Dynamics shell and coil NCHE. Geometric specifications for the concentric tube counter flow heat exchanger are listed in Table A.2.

Table A.2 Geometric Specifications for Concentric Tube Counterflow HX

L_{HX}	1 m
D_i	0.01905 m
D_o	0.03810 m
inner wall thickness	0.002 m

The heat exchanger inlet and outlet minor loss coefficients, fittings, and pipe dimensions and system parameters are the same for both heat exchangers, and are presented in Section 6.1.1. As the heat transfer surface area of the concentric tube counterflow heat exchanger was found to be very small ($0.0724\ m^2$) compared to the heat transfer surface area of the shell and coil heat exchanger ($0.5932\ m^2$), the concentric tube counterflow heat exchanger performed significantly worse than the shell and coil model. Figures A.3-4 presents the heat transfer rate and water flow rate of the heat exchangers, respectively, as a function of time, for April 1. Table A.3 presents April simulation results for the two heat exchangers.

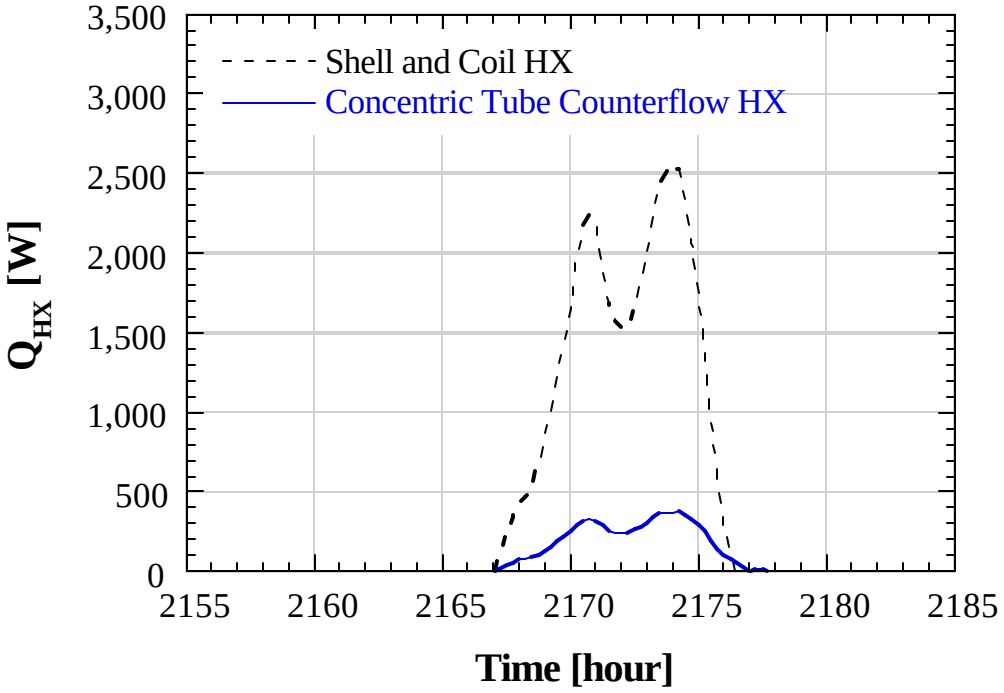

Figure A.3 Comparison of heat transfer rate as a function of time for shell and coil and concentric tube counterflow heat exchangers for April 1.

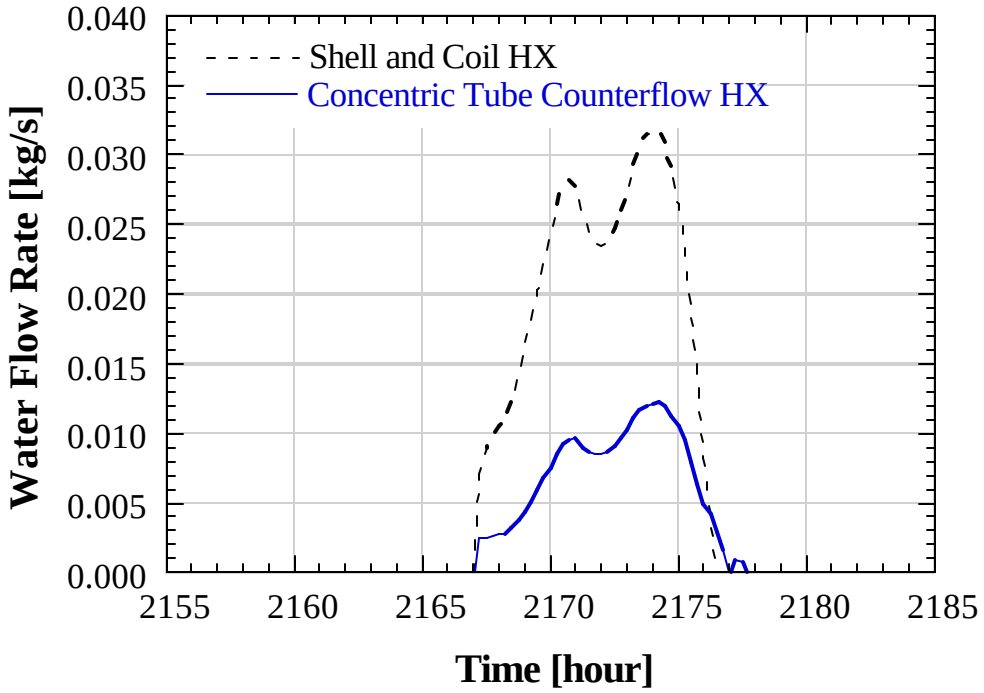

Figure A.4 Comparison of water flow rate as a function of time for shell and coil and concentric tube counterflow heat exchangers for April 1.

Table A.3 Solar Fraction for Concentric Tube Counterflow and Shell and Coil Heat Exchangers for April Simulations

Heat Exchanger	Solar Fraction
Shell and Coil	0.535
Concentric Tube Counterflow	0.134